Influence of Contact Geometry on Local Friction Energy and Stiffness of Revolute Joints

Alexander Gummer
Research Assistant
e-mail: gummer@mv.uni-kl.de

Bernd Sauer
Professor
e-mail: sauer@mv.uni-kl.de

University of Kaiserslautern,
Institute of Machine Elements,
Gears, and Transmissions,
Gottlieb-Daimler-Strasse
67663 Kaiserslautern, Germany

Revolute joints (also called pin joints or hinge joints) are used in many different mechanical systems such as robotic arms, door hinges, folding mechanisms, or hydraulic shovels. Since they transmit forces and give a rotational degree of freedom to the connected parts, revolute joints have a major impact on the dynamic behavior of the system into which they are built. Two main characteristics of these elements are their stiffness and their clearance. Both of them change as the wear between the joint's pin and the rod hole increases during operation. In order to consider these aspects in a multibody simulation an analytical, numerically effective method has been developed to calculate the stiffness of a revolute joint in dependence of the geometry and the wear state. In addition, the calculation algorithm allows for for the analysis of the local friction energy that occurs in the contact zone. In this paper, the calculation approach is presented together with the results for two different steady loaded revolute joints. [DOI: 10.1115/1.4006248]

Keywords: revolute joint, pin joint, hinge joint, clearance, friction energy, stiffness, wear

1 Introduction

Revolute joints are used in many mechanical systems and are the most common joints, according to Ref. [1]. Contrary to the ideal joints that are implemented in all commercial multibody simulation software, real joints have a clearance between the pin and the rod hole and are, therefore, considered as nonideal. The clearance influences the guidance accuracy, the dynamic behavior, and the loads in the contact zone of the joint. Many researchers have already investigated these nonideal joints and pointed out how important it is to consider the clearance in a dynamic simulation. In general, there are three different approaches for modeling the clearance: the massless link approach, the spring-damper approach, and the colliding bodies approach, where the two bodies are modeled as colliding bodies.

In the massless link approach, the pin and the rod hole are connected with a rigid massless link that has the length of the joint's clearance. This approach is used by Su et al. to calculate the contact forces in a slider-crank mechanism with a clearance joint [2]. The kinematics and forces are then transferred to a finite element method (FEM) model, in which the wear of the pin and rod hole is calculated. Therefore, the Archard wear law is used, which is calibrated with experimental data obtained from a pin on disk tribometer. The results from the calculation correlate quite well with the results from a wear experiment on a real slider-crank mechanism. Although the massless link approach considers the pin and the rod hole as always being in contact, Bu et al. found a way to detect detachment [3]. Therefore, they evaluate the tensile force in the link. If this force is approximately zero, they assume that the pin and rod hole are detached.

In the spring-damper approach the joint's parts are connected with a Kelvin-Voigt element to simulate the surface elasticity, as used in Refs. [4,5]. According to Refs. [6,7], the major drawbacks of this model are that the clearance is not really considered and the stiffness and damping parameter are difficult to quantify for different geometries.

In the colliding bodies approach the pin and the rod hole of the joint can move freely within the clearance. Outside the clearance zone a force constraint is applied. That's why this approach is also called the contact force approach. This is considered the most accurate of the presented approaches [7] and is therefore widely used. Flore et al. investigated the influence of five different contact force models on the dynamic behavior of a slider-crank mechanism [6]. The models are all based on the Hertzian theory and lead to similar results both in terms of pin trajectory and crank movement. A remarkable conclusion is that Lankarani and Nikravesh's force law, originally developed for spherical contacts, works quite well for line contacts when corrected with a pseudostiffness parameter. Later, they expand their model towards friction by implementing Coulomb's friction law. Different methods for describing the friction coefficient in dependence of the relative velocity are investigated. In Ref. [8] Flores also considers wear by implementing the law of Archard. This law gives a correlation between the wear volume and the contact force with the help of a wear coefficient that has to be empirically determined. Subsequently, the influence of lubrication on the dynamic behavior of the joint is considered [9]. A parametric study is presented that shows the huge impact of the clearance size on the dynamic load and the overall system behavior [10]. According to the authors, the stiffness of the links also has an influence, but is not yet considered. In Ref. [11] an impact force model is compared with the Hertzian theory for the dynamic analysis of a revolute joint with clearance in a slider-crank mechanism. Both models show similar results. The authors also investigate a lubricated joint, for which the peaks in the contact force are much lower. In Ref. [1], the contact models are further investigated. According to the authors, the Hertzian theory is only suitable for joints with large clearance, and the contact model of Persson can only be applied for small clearances. The limitations result from the assumptions upon which the different models are based. Due to these limitations, the authors use the FEM to calculate the contact. For a revolute joint with a rod hole diameter of 100 mm they calculate the stiffness for different clearances and compare the FE results with the results obtained with the Hertzian theory. For a clearance of 1 mm the two results correlate quite well, while for 0.1 mm the results from the Hertzian theory are totally out of range. They further develop an elastic foundation model for describing the contact of

Contributed by the Tribology Division of ASME for publication in the JOURNAL OF TRIBOLOGY. Manuscript received August 4, 2011; final manuscript received February 21, 2012; published online April 10, 2012. Assoc. Editor: Daniel Nélias.

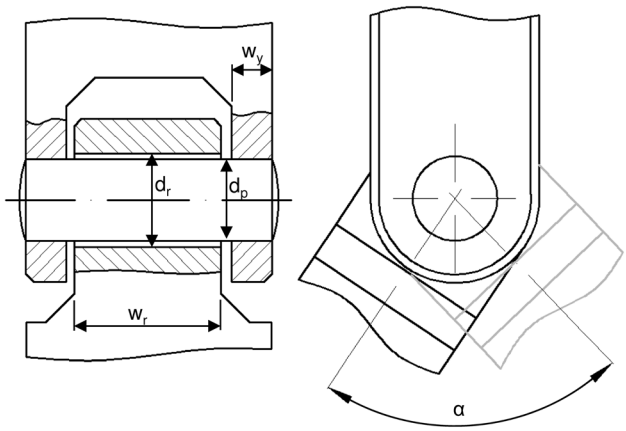

Dimensions

	Joint A	*Joint B*
w_y	50 mm	70 mm
d_p	80 mm	80 mm
d_r	80.2 mm	80.2 mm
w_r	120 mm	200 mm

Operating conditions

α	90°
f	0.2 Hz
Q	700 kN
sliding velocity	0.025 m/s 90.74 m/h

Fig. 1 Layout, dimensions, and operating conditions of the investigated joints

clearance joints that is valid for both large and small clearances. The new model fits the FE results quite well and much better than the Hertz or Persson models. Mukras et al. present a method to calculate the wear in a slider-crank mechanism [12]. The approach is similar to the one in Ref. [8]: The contact between the pin and the rod hole is calculated with a formula based on the Hertzian theory and, technically, is only valid for spherical contacts. The authors argue that the stiffness of this formula is similar to the stiffness formulas for line contacts, however much easier to implement in a numerical analysis. In addition, real line contact only occurs for exactly aligned cylinders. For the calculation of the wear, the Archard law is implemented. The calculated dynamic behavior and the wear are both compared with experimental results from a slider-crank apparatus and show a good correlation. Later, the authors compare the previously used contact force model to an elastic foundation model [13,14]. The latter is similar to the one used in Ref. [1]. Both models are capable of accurately calculating the contact force, the contact locations, and even the wear volume. Tian et al. implement the absolute nodal coordinate formulation to consider the elasticity of the connecting links in mechanisms with clearance joints [15]. Those joints are modeled with Lankarani and Nikravesh's continuous force law and Coulomb's friction law. For lubricated joints, they consider hydrodynamic effectsas in Ref. [9]. Their method is applied to two different examples: A double pendulum in the gravity field and a slider-crank mechanism. The authors conclude that the model with flexible links and lubrication leads to much lower impact forces. In Ref. [16], different continuous contact models are investigated in terms of their suitability for the calculation of conformal and nonconformal contacts. Especially for the conformal contacts, such as in journal bearings or roller chain drives, the authors recommend the contact models of Johnson and Radzimovsky. Lankarani and Nikravesh's widely used contact model shows the largest deviation and is thus explicitly not recommended. Megahed and Haroun present a model for mechanisms with multiple clearance joints under the SolidWorks/CosmosMotion software [7]. For the contact calculation, Lankarani and Nikravesh's continuous contact model and Coulomb's friction law are used. They compare the dynamic behavior of a slider-crank mechanism with ideal joints with the same mechanism with two clearance joints. As other previous authors have found, they detected higher force peaks due to impacts that are caused by the clearance.

In most papers that deal with the calculation of the wear in revolute joints, the wear depth leads to an increasing clearance between the pin and rod hole, while changes in the rod hole's profile are not considered. However, a changing profile influences the contact stiffness, the pressure distribution, and the wear progress. Therefore, a method is presented in this paper to calculate the stiffness of the pin-rod hole contact in dependence of the geometry of new and worn rod holes. The worn profiles are calculated

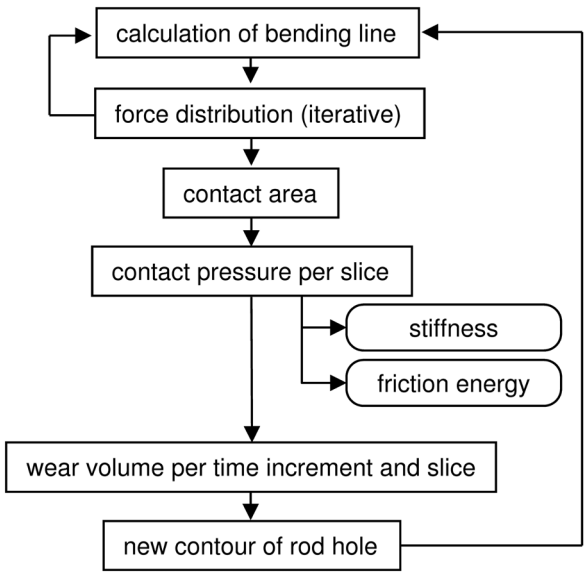

Fig. 2 Algorithm for calculating wear, stiffness, and friction energy of revolute joints

by applying Archard's wear law to the algorithm. The influence of lubrication, as investigated, for example, in Refs. [9,15], is neglected here. Instead, a friction coefficient for boundary lubrication is chosen, assuming that there is enough lubrication to cool the contact zone. In order to demonstrate the functionality offered by the new method, two joints have been chosen upon which to run calculations. Their main dimensions and the operating conditions are presented in Fig. 1. When used in machinery, the joint is subject to a dynamic load and different acting angles. Since the calculation algorithm presented is not yet implemented into a multibody simulation, the first calculations have been run with a simple steady state loadcase, where the load Q is constant and the rod is moved with a constant velocity, resulting from a constant acting angle α and frequency f.

2 General Approach

The principle of the calculation is shown in Fig. 2. In order to calculate the friction energy, the stiffness, and the wear of a revolute joint, the force and pressure distribution and the resulting penetration between the pin and the rod hole must be calculated. Since the contact zone depends on the bending line of the pin, the shape of the rod hole, and the load on the joint, conventional

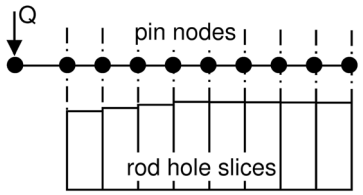

Fig. 3 Discretization of the pin and rod hole

calculation approaches for line contacts, e.g., Tripp's formulas [17], are not sufficient.

For the calculation of line contacts in roller bearings, slicing approaches are commonly used, where the rolling element is divided in a discrete number of slices along its axis and contact laws are applied on every single slice [18]. With this method the contact between a cylindrical bearing ring and the noncylindrical rolling element can be calculated. The slicing method is also applicable for the calculation of contact forces in revolute joints. Therefore, the rod hole and the pin are cut into matching slices. In order to calculate the bending line of the pin the finite element method is used. The pin is thereby discretized with beam elements along its axis. Every slice of the pin is then represented by a node in the FE-model and the forces calculated between the slices are applied on the nodes, respectively (cf., Figure 3). The distribution of the contact force influences the bending line and vice versa. In order to find a solution where the bending line and force distribution fit together, an iterative algorithm was implemented in the calculation. First, the bending line is calculated with an assumed load distribution. Then the bended pin is assumed to be stiff and the corresponding load distribution is determined, which is also an iterative process. With this load distribution a new bending line is calculated for which the corresponding load distribution is again determined. This procedure is repeated until the changes in the bending line and load distribution do not exceed a defined error tolerance. Further details on the FEM used in this paper and the contact force calculation can be found in Sect. 3.

After the contact calculation is finished, the contact area and, considering the force, the contact pressure of every single slice are calculated. Now the overall stiffness of the joint and the local friction energy can be determined. Details about these calculations are presented in the corresponding sections of this paper. The contact pressure is further used to calculate the wear volume. Therefore, an empirical wear calculation approach is used (cf., Sec. 6). With a previously calculated relation between the wear volume and the wear depth, the new contour of the rod hole can be calculated. This new contour is then used for the calculation of the bending line of the pin in the next time step.

3 Contact Calculation

3.1 Finite Element Method for Bending Line. For the calculation of the bending line of the pin, the latter is discretized by beam elements according to the finite element method. The element stiffness matrix for such elements is as follows

$$EI \cdot \begin{bmatrix} \frac{12}{l^3} & \frac{-6}{l^2} & \frac{-12}{l^3} & \frac{-6}{l^2} \\ \frac{-6}{l^2} & \frac{4}{l} & \frac{6}{l^2} & \frac{2}{l} \\ \frac{-12}{l^3} & \frac{6}{l^2} & \frac{12}{l^3} & \frac{6}{l^2} \\ \frac{-6}{l^2} & \frac{2}{l} & \frac{6}{l^2} & \frac{4}{l} \end{bmatrix} \tag{1}$$

In the matrix, E is the Young's modulus, I is the second moment of inertia, and l is the length of the beam element, which is the same as the length of one slice. With the stiffness matrix of the single elements, the overall stiffness matrix K can be built, with which the basic system of equations of the FEM can be created, together with the force vector F and the displacement vector U

$$K \cdot U = F \tag{2}$$

For solving this system of equations, the stiffness matrix is inverted and multiplied with both sides of the equation. The result of this operation is the displacement vector U, which is then used for the calculation of the bending line of the pin. Since the pin is symmetrical the calculation can be accelerated by calculating only half of the pin and using the appropriate boundary conditions. With this approach, a good correlation to the analytically calculated bending lines can be achieved, even with only few elements. In the calculations presented in this paper, 24 elements were used to discretize the half pin, resulting in an element size of 5 mm for joint A and 8.3 mm for joint B. Higher element numbers increase the computational effort but do not greatly affect the results. For more details on the FEM, please refer to literature on this topic, such as Refs. [19,20].

When the clearance of the joint is low and the loads are high, the pin contacts the rod hole on the back side, as schematically shown in Fig. 4. In this case, the calculation of the bending line and contact forces is not working, as previously described.

Therefore, a different approach was chosen: When contact is detected on the back side of the pin, the displacements of the affected nodes are set to a fixed value, as if the backside contact was unlimited stiff. Then the bending line is calculated again with this new boundary condition. To implement this approach into the calculation, the system of equations has to be modified as follows. If the system of equations is

$$\begin{bmatrix} K_{11} & K_{12} & K_{13} & K_{14} & K_{15} & K_{16} \\ K_{21} & K_{22} & K_{23} & K_{24} & K_{25} & K_{26} \\ K_{31} & K_{32} & K_{33} & K_{34} & K_{35} & K_{36} \\ K_{41} & K_{42} & K_{43} & K_{44} & K_{45} & K_{46} \\ K_{51} & K_{52} & K_{53} & K_{54} & K_{55} & K_{56} \\ K_{61} & K_{62} & K_{63} & K_{64} & K_{65} & K_{66} \end{bmatrix} \cdot \begin{bmatrix} U_1 \\ U_2 \\ U_3 \\ U_4 \\ U_5 \\ U_6 \end{bmatrix} = \begin{bmatrix} F_1 \\ F_2 \\ F_3 \\ F_4 \\ F_5 \\ F_6 \end{bmatrix} \tag{3}$$

and the displacement of the 3rd node shall be set to $U_5 = a$, then the modified system is

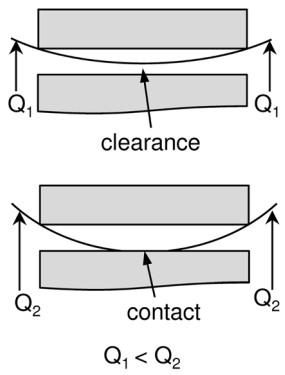

Fig. 4 Single side and double side contact between the pin and rod hole

Table 1 Continuous force models for calculation of conformal contacts (bodies of the same material)

Hertz [1]

$$\delta = \frac{2 \cdot L}{\pi \cdot E} \cdot \left[\ln\left(\frac{\pi \cdot E \cdot \Delta r}{L} \right) - 1 \right] \tag{15}$$

Johnson [16]

$$\delta = \frac{L}{\pi \cdot E^*} \cdot \left[\ln\left(\frac{4 \cdot \pi \cdot E^* \cdot \Delta r}{L} \right) - 1 \right] \tag{16}$$

Radzimovsky [16]

$$\delta = \frac{L}{\pi \cdot E^*} \cdot \left[\frac{2}{3} + \ln\left(\frac{2 \cdot d_r}{b} \right) + \ln\left(\frac{2 \cdot d_p}{b} \right) \right] \tag{17}$$

$$b = 2.15 \cdot \sqrt{\frac{L \cdot R}{E}}$$

$$R = \frac{r_r \cdot r_p}{r_r - r_p}$$

Lankarani & Nikravesh [16]

$$\delta = \left(\frac{3 \cdot Q}{4 \cdot \pi \cdot E^* \cdot \sqrt{R}} \right)^{1/n} \tag{18}$$

n = 1.0 to 1.5; R according to Eq. (17)

Persson [1]

$$\frac{E \cdot \Delta r}{L} = \frac{2 - [\log(b^2 + 1) + 2 \cdot b^4]}{\pi \cdot (b^2 + 1) \cdot b^2} \tag{19}$$

$$b = \tan\left(\frac{\varepsilon}{2} \right)$$

$$\cos(\varepsilon) = \frac{\Delta r}{\Delta r + \delta}$$

Liu [1]

$$L = \frac{1}{2} \cdot \pi \cdot \delta \cdot E \cdot \sqrt{\frac{\delta}{2 \cdot (\Delta r + \delta)}} \tag{20}$$

all equations with

$$\Delta r = r_r - r_p \tag{21}$$

$$E^* = \left(\frac{E}{2 \cdot (1 - \upsilon^2)} \right)$$

$$\begin{bmatrix} K_{11} & K_{12} & K_{13} & K_{14} & 0 & K_{16} \\ K_{21} & K_{22} & K_{23} & K_{24} & 0 & K_{26} \\ K_{31} & K_{32} & K_{33} & K_{34} & 0 & K_{36} \\ K_{41} & K_{42} & K_{43} & K_{44} & 0 & K_{46} \\ 0 & 0 & 0 & 0 & 1 & 0 \\ K_{61} & K_{62} & K_{63} & K_{64} & 0 & K_{66} \end{bmatrix} \cdot \begin{bmatrix} U_1 \\ U_2 \\ U_3 \\ U_4 \\ U_5 \\ U_6 \end{bmatrix} = \begin{bmatrix} F_1 - a \cdot K_{15} \\ F_2 - a \cdot K_{25} \\ F_3 - a \cdot K_{35} \\ F_4 - a \cdot K_{45} \\ a \\ F_6 - a \cdot K_{65} \end{bmatrix} \tag{4}$$

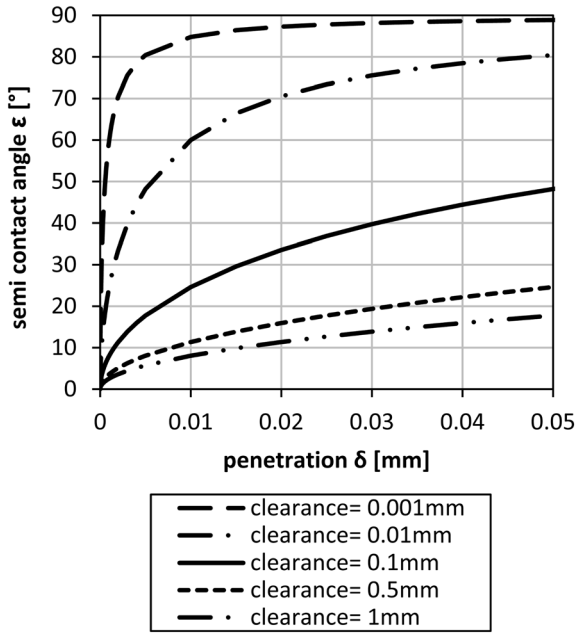

Fig. 6 Influence of the penetration on the semi-contact angle for different values of clearance

This system can be further reduced by removing the 5th line and column. Please refer to literature such as Refs. [19,21] for more details.

3.2 Contact Force. As shown in Sec. 1, there are several continuous contact models that are used for conformal contacts. Table 1 shows the formulas of six different approaches, taken from Refs. [1,16]. Note that in most models a load per cylinder length (L) is used, while in Lankarani and Nikravesh's model the contact force Q is used. That means the length of the cylinders does not influence the contact force in this model. This can also be seen in Fig. 5, where the different contact models are applied on the two joints. For the investigations in this paper, the contact force model according to Liu et al. (Eq. (20)) is used, due to the good results presented in Ref. [1] and its simplicity.

3.3 Contact Area. Liu et al. [1] use Persson's formula (Eq. (19)) to calculate the semi-contact angle ϵ. In this formula, the angle is independent from the absolute values of the radii of the contacting bodies, but depends only on the clearance and penetration. This relation is illustrated in Fig. 6 for different clearances. With the semi-contact angle, the contact area is calculated by

$$A = (r_r + r_p) \cdot \varepsilon \cdot l \tag{5}$$

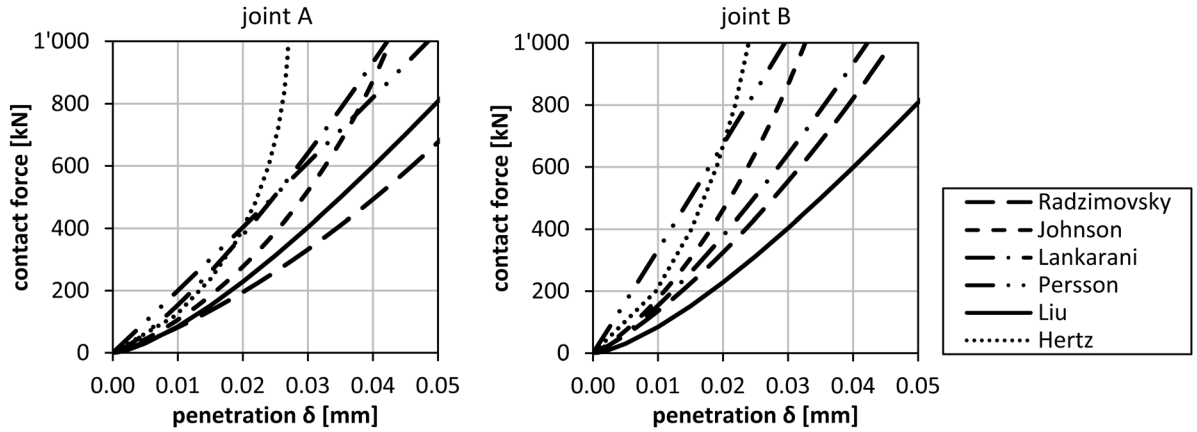

Fig. 5 Comparison of contact force models for investigated joints, when the pin is stiff

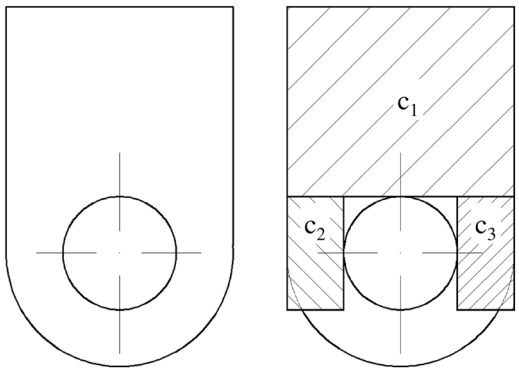

Fig. 7 Simple approach to calculate the stiffness of the rod and the yoke

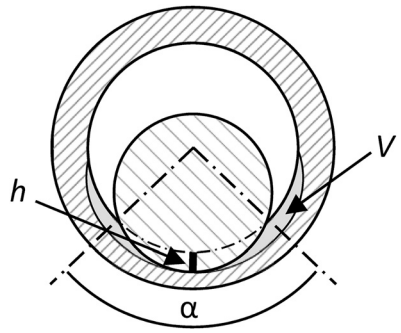

Fig. 8 Calculation of the wear volume, assuming that the complete wear is on the bush

where l is the length of the slice. This formula is used in this paper to calculate the contact area.

4 Friction Energy

With the load distribution in the contact zone of the revolute joint, the local friction energy can be calculated. In general, the frictional power is determined as follows [22]

$$P = \iint \mu \cdot p(x,y) \cdot v_{rel}(x,y) dxdy \tag{6}$$

The pressure p is a result of the contact calculation (see Fig. 2), whereas the velocity v_{rel} between the pin and rod hole is given by the working conditions of the joint. As previously mentioned, the friction coefficient μ is chosen from the boundary lubrication regime. For the calculations conducted in this paper a value of 0.1 was used. Assuming that the pressure distribution on one single slice and the relative velocity is constant, the frictional power per slice can be more easily calculated by the following formula

$$P_s = \mu \cdot p_s \cdot v_{rel} \tag{7}$$

In order to obtain the friction energy, the frictional power must be integrated over time

$$W = \int P dt \tag{8}$$

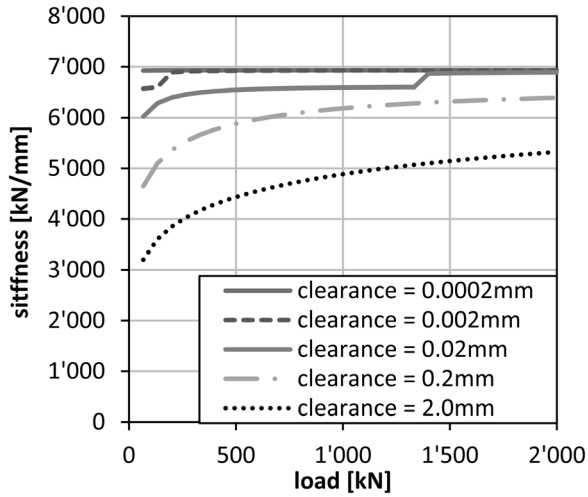

Fig. 9 Influence of the joint clearance on the load depending on stiffness (joint A)

If the velocity v_{rel} is constant, the friction energy is

$$W_s = \mu \cdot p_s \cdot v_{rel} \cdot t \tag{9}$$

where t is the considered period of time.

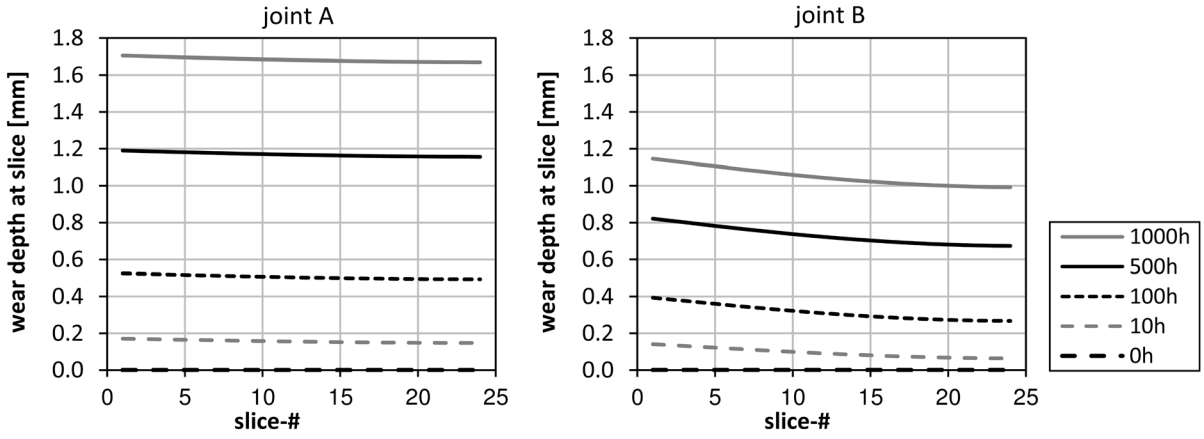

Fig. 10 Wear depths of joints A and B at different time steps (Remarks: the slices of joint B are wider than the slices of joint A; slice #24 is in the middle of the pin; wear coefficients: $C = 1 \times 10^{-20}$ and $m = 1.1$; operating conditions are as presented in Fig. 1)

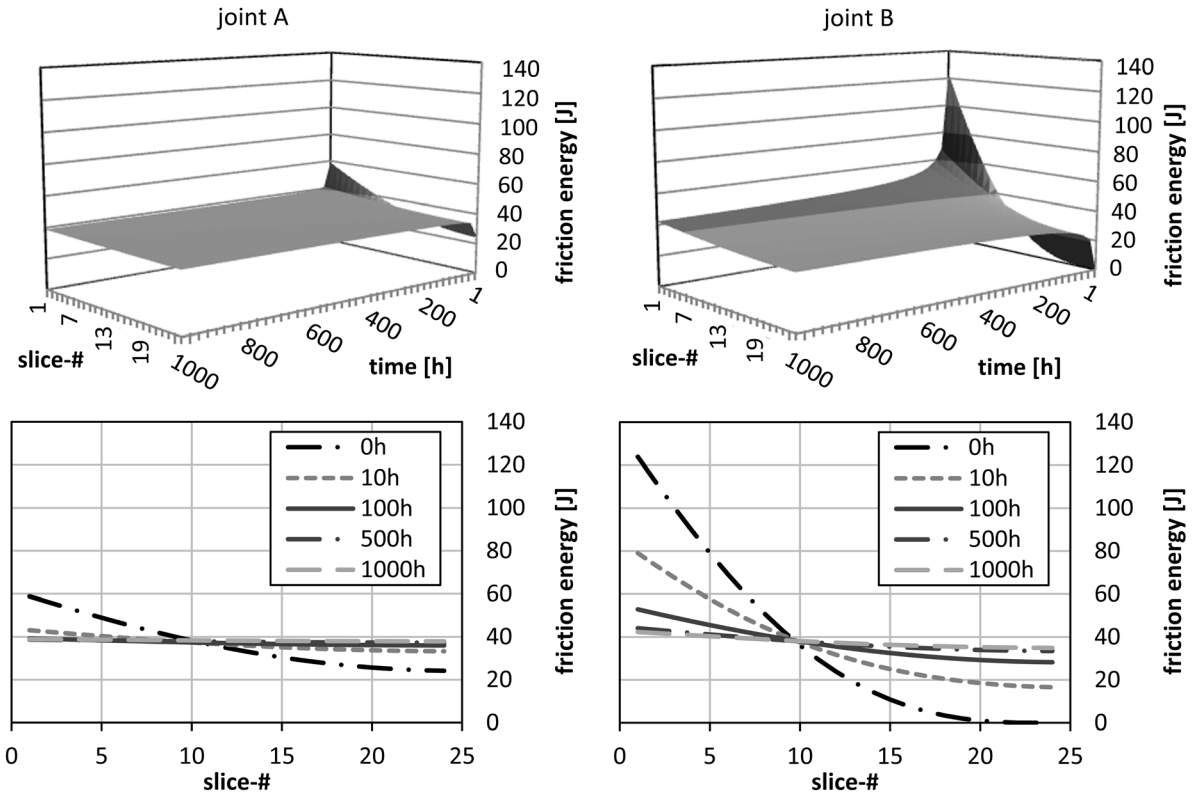

Fig. 11 Local friction energy at slices for different wear states and a time period of 1 s (Remarks: the slices of joint B are wider than the slices of joint A; slice #24 is in the middle of the pin; wear coefficients: $C = 1 \times 10^{-20}$ and $m = 1.1$; operating conditions are as presented in Fig. 1; $\mu = 0.1$)

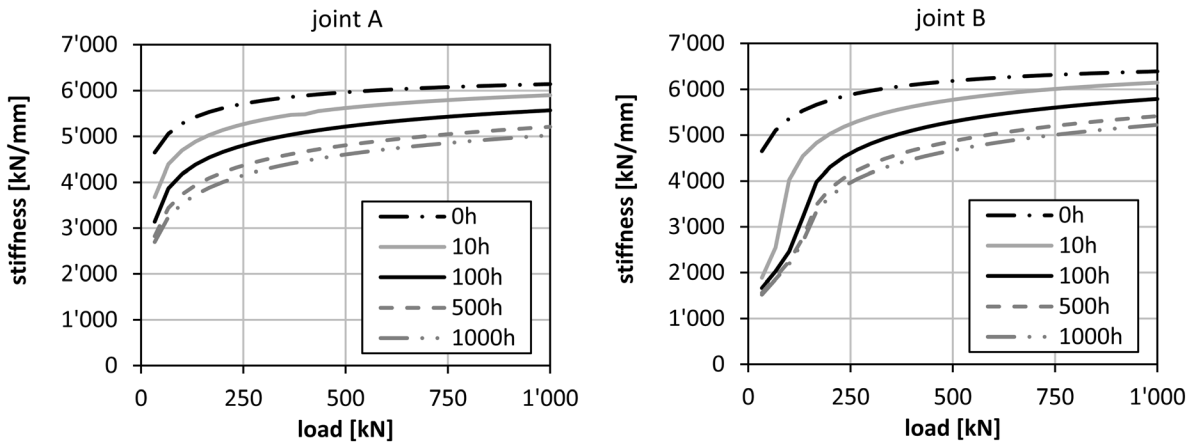

Fig. 12 Load depending on the stiffness of revolute joints for different wear states (wear coefficients: $C = 1 \times 10^{-20}$ and $m = 1.1$; operating conditions as presented in Fig. 1)

5 Joint Stiffness

The stiffness of a revolute joint is mainly composed of the stiffness of the yoke (c_y), the stiffness of the rod (c_r), the bending stiffness of the pin (c_p), and the stiffness of the press fit between the pin and the yoke. The latter is neglected in this paper. The stiffness of the rod and the stiffness of the yoke are both approximated by the stiffness of three rectangular bodies, as shown in Fig. 7. Accordingly, the formula is

$$c_r = \left(\frac{1}{c_1} + \frac{1}{c_2 + c_3} \right)^{-1} \tag{10}$$

The overall stiffness of the joint (c_j) is then calculated by

$$c_j = c_r + c_y + c_p \tag{11}$$

6 Wear Volume and Wear Depth

Wear is the advancing loss of material out of a surface of a body, caused by a tribological load. There are four basic wear mechanisms that normally appear in combination: adhesion, abrasion, surface fatigue, and tribochemical reactions [23]. According to Ref. [24], adhesion and abrasion are the dominant mechanisms in a journal bearing that runs in the area of mixed lubrication. Kinematically, such a bearing is similar to a revolute joint. For the calculation of wear, many different approaches can be found. Meng and Ludema declare that they found 182 wear equations [25]. The most widely spread wear equation tracks back to

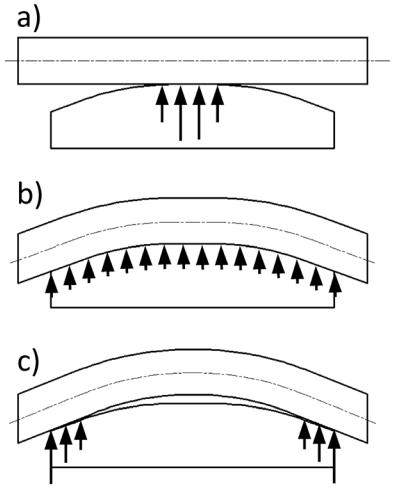

Fig. 13 Different contact conditions depending on the load of the joint

Archard and is used by many researchers for the calculation of wear in revolute joints [2,8,12–14]

$$V = C \cdot \frac{Q}{H} \cdot s \tag{12}$$

In this equation, V is the volumetric amount of wear, C is the empirically determined wear coefficient, Q is the contact force, H is the hardness of the softer contact partner, and s is the sliding distance. Many authors propose slightly modified equations, e.g., for integrating the surface hardness into the wear coefficient and considering a nonlinear load dependency. Such an equation can be found in Ref. [26]

$$V = C \cdot Q^m \cdot s \tag{13}$$

Here, V is again the wear volume, C is an empirically determined wear coefficient, Q is the contact force, s is the sliding distance, and m is a wear exponent that accounts for the nonlinear influence of the load and has to be empirically determined. Due to the bending line of the pin and the small clearances in the investigated joints, the contact area is drastically varying. Thus, the contact area must be considered in the wear equation. Therefore, Eq. (13) is modified as follows

$$V = C \cdot \left(\frac{Q}{A}\right)^m \cdot s \tag{14}$$

In this equation, V is the wear volume, C is an empirically determined wear coefficient, Q is the contact force, A is the contact area, s is the sliding distance, and m is a wear exponent. The values for the wear coefficients used in this paper are: $C = 1 \times 10^{-20}$ and $m = 1.1$. For the calculation of the wear depth, it is assumed that the complete wear occurs in the rod hole, thus provoking an increase in clearance. This is not valid for every revolute joint, but can occur, e.g., in chain joints, as shown in Ref. [27]. For the calculation of the pin wear and the resulting pin shape, a discretization of the pin is necessary, as shown in Ref. [8]. Such a discretization is not yet implemented in the calculation algorithm. Instead, the correlation between the wear volume V, the wear depth h, and the acting angle α, as shown in Fig. 8, is used.

7 Results

7.1 Influence of the Joint Clearance on the Stiffness. According to the chosen contact model, the stiffness of the joint increases if the clearance decreases. This effect is shown in Fig. 9 for joint A. For a rather large clearance of 2.0 mm, the stiffness varies between 3′200 and 5′500 kN/mm, depending on the load. If the clearance is reduced to 0.2 mm, the stiffness increases, being between 4′600 and 6′300 kN/mm. For a clearance of 0.02 mm and a force greater than 1′400 N, the backside of the pin comes in contact with the rod hole (cf., Fig. 4). In this moment, the stiffness rapidly increases. If the clearance is further reduced, the backside contact occurs for smaller loads. The small clearances and high loads shown in Fig. 9 are surely not relevant for the investigated joint, however, this might affect those with other geometries.

7.2 Influence of Geometry and Wear on Friction Energy and Stiffness. With the data presented in Fig. 1, a complete calculation, as shown in Fig. 2, was run on the two joints. The result of the wear calculation is presented in the following figures. The diagrams in Fig. 10 show the wear depth at each slice for different wear times, which visualizes the inner profile of the rod hole. As explained earlier, the calculation is reduced to the half pin to accelerate the computation. For that reason the results are also only shown for the half pin, whereas slice #24 represents the middle of the joint. Due to the wider slices, the wear depths of joint B are smaller for the same wear volume. Since the bending of the pin is also bigger in joint B, the rod profile is more curved than in joint A. This results in a greater diversification of the local friction energy, as shown in Fig. 11. The global load on the two joints is the same, so that the sums of the friction energies are also similar. Both diagrams show that with progressing wear, the friction energies become more equally distributed among the slices. Since the friction energies and the forces are directly correlated, the forces also become equally distributed.

In Fig. 12, the stiffness of the joints at the different wear states are presented. Without any wear of the rod (“0 h”) the stiffness of joint B is slightly higher than that of joint A. When the rod becomes worn out, the stiffness decreases due to the increasing clearance. In addition to that, the stiffness of joint B becomes lower than the stiffness of joint A for small loads. The reason for this is the profile of the worn rod that is more curved in joint B (cf., Figure 10). These results demonstrate the huge impact of wear on the stiffness of a joint.

The reason for the load dependency is the different contact conditions that change with the external load. This is illustrated in Fig. 13. At a small load (Fig. 13(*a*)), the pin only contacts the rod in the middle, giving lots of the free length of the pin that is subject to bending. As the load on the pin increases, the contact area also increases, leaving less free length of the pin and, thus, increasing the stiffness of the joint. When the pin is completely in contact with the rod (Fig. 13(*b*)), the gradient of the stiffness changes and the stiffness itself becomes less dependent on the external load. Another change in the stiffness gradient can be expected when the load is high enough to lift the pin in the middle, so that the load is only supported at the edge of the rod (Fig. 13(*c*)).

In Fig. 14, the forces at each slice for different loads on the worn profiles of the joints after 1000 h (cf., Figure 10) are presented. For a small load, the pin of joint B is only in contact with the middle of the rod (slice #24). The higher the loads, the more slices are in contact. In joint A all slices are in contact, even for smaller loads; thus, the joint stiffness is less dependent on the wear state. The results show that the contact state that is presented in Fig. 13(*c*) is outside the reasonable load spectrum of the investigated joints.

So far, no experimental data is available to compare the results of the calculation, neither by our own experiments nor in other publications. Nevertheless, the results show that the load dependency of revolute joints should not be neglected, since it changes the contact stiffness and, thereby, the reaction forces in the system. Besides the clearance, the load dependent stiffness should,

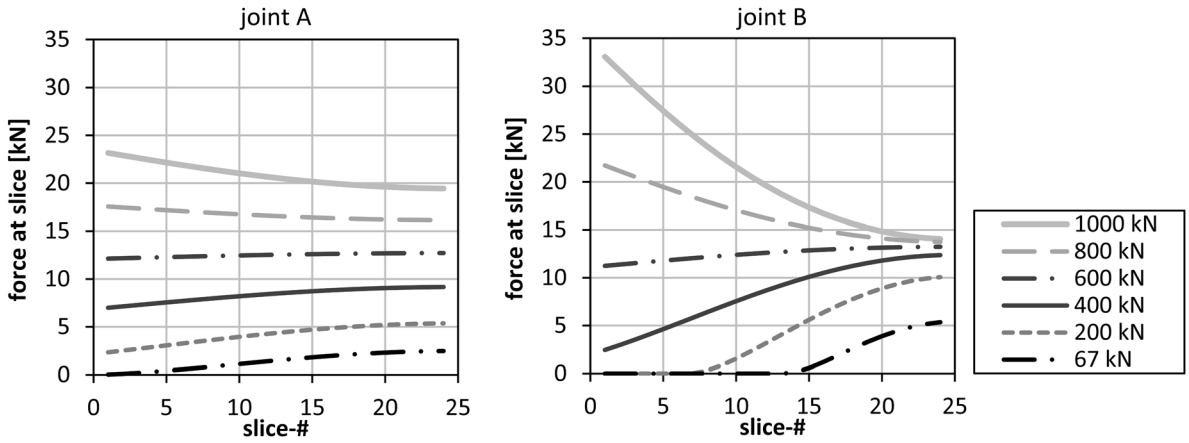

Fig. 14 Force at different slices for different loads on the worn profile after 1000 h (wear coefficients: $C = 1 \times 10^{-20}$ and $m = 1.1$; operating conditions are as presented in Fig. 1)

therefore, be considered when calculating the influence of a revolute joint on the dynamic behavior of an entire system.

8 Conclusions

In this paper, a method for calculating the local friction energy and the stiffness of revolute joints with different geometry is presented. Furthermore, the calculation of the wear in the contact zone of the pin and rod hole, similar to the law of Archard, is implemented. With the local friction energy, not only the energy loss during operation can be calculated, it can also be used to implement more sophisticated wear laws in the future.

The whole method is based on the slicing techniques that are commonly used for calculating line contacts, e.g., in roller bearings. The slicing technique is combined with an FE beam algorithm for the calculation of the bending line of the pin. This enables the determination of the contact conditions with high accuracy and for basically all possible geometries and wear profiles. In addition, an approach for calculating a two-sided contact between the pin and rod has been implemented, however, the results show that this contact condition is of only minor importance for revolute joints in practice.

The first results of the method are presented in the last section of the paper, showing not only the variety of possibilities, but also the huge impact of the wear on the stiffness characteristics. This is caused by the different contact conditions for the different external loads. Therefore, the load dependent stiffness should be considered in all dynamic analyses of systems with revolute joints.

Nomenclature

The units used throughout the paper are based on SI standards. In case an exception was made, the unit was explicitly specified throughout the paper.

a = displacement at node (m)
A = contact area (m^2)
b = half width of contact area/tangents of half ε(m)
c = stiffness (N/m)
C = wear coefficient (usually K is used for the wear coefficient, however, it is replaced here to avoid confusion with the stiffness matrix)
d = diameter (m)
E = Young's modulus (N/m^2)
f = frequency (Hz)
F = force vector
h = wear depth (m)
H = hardness of softer contacting body (N/m^2)
I = second moment of inertia (m^4)
K = stiffness matrix
l = length of slice or beam element (m)
L = load per length (N/m)
m = wear exponent
n = exponent in Lankarani and Nikravesh's contact model
p = contact pressure (N/m^2)
P = frictional power (W)
Q = load (N)
r = radius (m)
R = relative curvature of contact
s = sliding distance (m)
t = time (s)
U = displacement vector
v_{rel} = relative velocity of contacting bodies (m/s)
V = wear volume (m^3)
w = width (m)
W = friction energy (J)
x = contact area longitudinal direction (m)
y = contact area transverse direction (m)
α = acting angle (°)
δ = penetration (m)
Δr = radius based clearance (m)
ε = semiangle of contact (rad)
μ = coefficient of friction
ν = Poisson's ratio

Indices

j = joint
p = pin
r = rod
s = slice
y = yoke

References

[1] Liu, C.-S., Zhang, K., and Yang, R., 2007, "The FEM Analysis and Approximate Model for Cylindrical Joints With Clearance," Mech. Mach. Theory, **42**, pp. 183–197.
[2] Su, Y., Chen, W., Tong, Y., and Xie, Y., 2010, "Wear Prediction of Clearance Joint by Integrating Multibody Kinematics With Finite-Element Method," J. Eng. Tribol., **224**(8), pp. 815–823.
[3] Bu, W., Liu, Z., Tan, J., and Gao, S., 2010, "Detachment Avoidance of Joint Elements of a Robotic Manipulator With Clearance Based on Trajectory Planning," Mech. Mach. Theory, **45**(6), pp. 925–940.
[4] Dubowsky, S. and Freudenstein, F., 1971, "Dynamic Analysis of Mechanical Systems With Clearances—Part 1: Formulation of Dynamic Model," ASME J. Eng. Ind., **93**(1), pp. 305–309.
[5] Dubowsky, S. and Freudenstein, F., 1971, "Dynamic Analysis of Mehanical Systems With Clearances—Part 2: Dynamic Response," ASME J. Eng. Ind., **93**(1), pp. 310–316.
[6] Flores, P. and Ambrosio, J., 2004, "Revolute Joints With Clearance in Multibody Systems," Comput. Struct., **82**, pp. 1359–1369.
[7] Megahed, S. M. and Haroun, A. F., 2012, "Analysis of the Dynamic Behavioral Performance of Mechanical Systems With Multibody Clearance Joints," ASME J. Comput. Nonlinear Dyn., **7**, p. 011002.
[8] Flores, P., 2009, "Modeling and Simulation of Wear in Revolute Clearance Joints in Multibody Systems," Mech. Mach. Theory, **44**(6), pp. 1211–1222.

[9] Flores, P., Ambrosio, J., Claro, J. C. P., Lankarani, H. M., and Koshy, C. S., 2009, "Lubricated Revolute Joints in Rigid Multibody Systems," ASME J. Tribol., **132**, p. 031604.
[10] Flores P., 2010, "A Parametric Study on the Dynamic Response of Planar Multibody Systems With Multiple Clearance Joints," Nonlinear Dyn., **61**, pp. 633–653.
[11] Schwab, A. L., Meijaard, J. P., and Meijers, P., 2002, "A Comparison of Revolute Joint Clearance Models in the Dynamic Analysis of Rigid and Elastic Mechanical Systems," Mech. Mach. Theory, **37**(9), pp. 895–913.
[12] Mukras, S., Kim, N. H., Mauntler, N. A., Schmitz, T. L., and Sawyer, W. G., 2010, "Analysis of Planar Multibody Systems With Revolute Joint Wear," Wear, **268**, pp. 634–652.
[13] Mukras, S., Mauntler, A., Kim, N. H., Schmitz, T. L., and Sawyer, W. G., 2010, "Evaluation of Contact Force and Elastic Foundation Models for Wear Analysis of Multibody Systems," Proceedings of the ASME 2010 International Design Engineering Technology Conferences, August 15-18, Montreal, Quebec, Canada, Paper No: DETC2010-28750.
[14] Mukras, S., Kim, N. H., Mauntler, N. A., Schmitz, T., and Sawyer, W. G., 2010, "Comparison Between Elastic Foundation and Contact Force Models in Wear Analysis of Planar Multibody System," ASME J. Tribol., **132**(3), p. 031604.
[15] Tian, Q., Zhang, Y., Chen, L., and Yang, J., 2010, "Simulation of Planar Flexible Multibody Systems With Clearance and Lubricated Revolute Joints," Nonlinear Dyn., **60**, pp. 489–511.
[16] Pereira, C. M., Ramalho, A. R., and Ambrosio, J. A., 2011, "A Critical Overview of Internal and External Cylinder Contact Force Models," Nonlinear Dyn., **63**, pp. 681–697.
[17] Tripp, J. H., 1985, "Hertzian Contact in Two and Three Dimensions," NASA Tech. Paper Ser., **2473**, pp. 1–24.
[18] Teutsch, R. and Sauer, B., 2004, "An Alternative Slicing Technique to Consider Pressure Concentrations in Non-Hertzian Line Contacts," ASME J. Tribol., **126**, pp. 436–442.
[19] Madenci, E. and Guven, I., 2006, *The Finite Element Method and Applications in Engineering Using ANSYS*, Springer, New York.
[20] Rieg, F. and Hackenschmidt, R., 2009, *Finite Elemente Analyse für Ingenieure*, Carl Hanser Verlag, München, Wien.
[21] Betten, J., 1998, *Finite Elemente für Ingenieure 1*, Springer, Berlin, Heidelberg, New York.
[22] Kümmerle, T., Wohlgemuth, M., Birkhofer, H., and Sauer, B., 2009, "The Use of Wear for Lifetime Prolongation of Solid Lubricated Ball Bearings," Proceedings of the ASME/STLE International Joint Tribology Conference, October 19-20, Memphis, Tennessee, USA.
[23] Mang, T., Bobzin, K., and Bartels, T., 2011, *Industrial Tribology*, Wiley-VCH, Weinheim.
[24] Habig, K.-H., 1980, *Verschleiß und Härte von Werkstoffen*, Carl Hanser Verlag, München, Wien.
[25] Meng, H. C. and Ludema, K. C., 1995, "Wear Models and Predictive Equations: Their Form and Contents," Wear, **181-183**, pp. 443–457.
[26] Bayer, R. G., and 1994, *Mechanical Wear Prediction and Prevention*, Marcel Dekker,New York.
[27] Gummer, A., Fábián, Cs., and Sauer, B., 2012, "Experimental Investigation of Roller Chain Wear," 18th International Colloquium Tribology, 10-12 January, Ostfildern, Germany.